

NJC

Accepted Manuscript



This is an *Accepted Manuscript*, which has been through the Royal Society of Chemistry peer review process and has been accepted for publication.

Accepted Manuscripts are published online shortly after acceptance, before technical editing, formatting and proof reading. Using this free service, authors can make their results available to the community, in citable form, before we publish the edited article. We will replace this *Accepted Manuscript* with the edited and formatted *Advance Article* as soon as it is available.

You can find more information about *Accepted Manuscripts* in the [Information for Authors](#).

Please note that technical editing may introduce minor changes to the text and/or graphics, which may alter content. The journal's standard [Terms & Conditions](#) and the [Ethical guidelines](#) still apply. In no event shall the Royal Society of Chemistry be held responsible for any errors or omissions in this *Accepted Manuscript* or any consequences arising from the use of any information it contains.

Synthesis, X-ray structural features, DFT calculations and fluorescence studies of a new pyridoxal-benzimidazole ligand and its respective molybdenum complex.

Mateus Brum Pereira¹, Cristiéli R. Kopp¹, Liniquer A. Fontana¹, Gelson Manzoni de Oliveira*¹, Davi Fernando Back*¹, Paulo C. Piquini², Marcos A. Villetti³

¹ Departamento de Química, Laboratório de Materiais Inorgânicos- LMI, Universidade Federal de Santa Maria, UFSM, 97115-900 Santa Maria, RS, Brazil.

² Departamento de Física, Universidade Federal de Santa Maria, UFSM, 97105-900 Santa Maria, RS, Brazil

³ Laboratório de Espectroscopia e Polímeros, Departamento de Física, Universidade Federal de Santa Maria, 97105-900 Santa Maria-RS, Brazil

* Corresponding authors. Tel.: 055-55-3220-8757; fax: 055-55-3220-8031.

E-mail addresses: manzonideo@smail.ufsm.br; daviback@gmail.com

Abstract.

Pyridoxal hydrochloride reacts with 1,2-phenylenediamine to give 4-(1H-benzimidazol-2-yl)-5-(hydroxymethyl)-2-methylpyridin-3-ol hydrochloride (BIMIPY, **1**). The reaction of **1** with bis(acetylacetonato)-dioxidomolybdenum(VI) leads to the formation of the complex $[(\text{MoO}_2)_2(\text{H}_2\text{O})_2(\mu\text{-O})(\text{BIMIPY-H}^+)_2]\cdot 4\text{DMSO}\cdot 2\text{H}_2\text{O}$ (**2**). In the binuclear complex the metal centers attain a distorted octahedral geometry; a water molecule coordinates to each Mo atom and two imidazolic ligands chelate two MoO_2^{+2} ions. The sixth coordination position in complex **2** is accomplished by a μ -oxido ligand, with an inversion center, which connects two moieties of $[(\text{MoO}_2)(\text{H}_2\text{O})(\text{BIMIPY-H}^+)]$ to a dinuclear species. Secondary, intermolecular hydrogen bonds support the growth of the supramolecular assembly of the Mo complex. Mechanisms for the formation of the functionalized benzimidazole ligand are also proposed and discussed. First principles DFT calculations of reactivity indexes are used to investigate a possible mechanism leading from the benzimidazole to a dimeric complex involving (MoO_2^{+2}) molecules and an oxido bridge ligand. Further, the expected fluorescence of the complex is absent, due to a decomposition of the complex in solution. On the other hand, an experimental investigation of the photophysical properties of the ligand shows that it is fluorescent. Time dependent density functional theory

calculations are performed to characterize the absorption and fluorescence spectra of the ligand.

Keywords: Pyridoxal; molybdenum , benzimidazole ligands

1. Introduction

The interest in the chemistry of coordination compounds involving vitamin B6 derivatives increased since Metzler and co-workers [1,2] appraised the biological potential of enzymes containing the active site pyridoxal phosphate in reactions of various amino acids and metal ions. These reactions include transamination [3], racemization [4], decarboxylation [5] and serine/threonine dehydratase [6,7]. Hence, for bioinorganic chemistry pyridoxal synthetic compounds are promising because they can act as catalysts in biochemical routes. There are several researches involving pyridoxal compounds with antiviral properties, as immunosuppressant, as selective apoptosis-inducing virus type 1 (HIV-1) [8], as well as in the interconversion of amino acids with metal ions to promote non-enzymatic reactions [9], in interactions of organometallic compounds of Sn^{IV} with vitamin B6 [10] and insulin-sensitizing agents [11].

Recently we have reported some reactions about the complexation of uranium and thorium with pyridoxal derivatives. The syntheses of these complexes and their structure elucidation, as far we are concerned, can

represent further qualitative contributions in the researches on possible models of interaction of radioactive and heavy elements with human beings [12–17].

Many benzimidazole derivatives are fluorescent molecules, as they are able to perform the ESIPT effect – excited state intramolecular proton transfer – which occurs in compounds having a donor group and an acceptor group of protons linked in a network. The occurrence of fluorescence depends upon the transfer of an acid proton (OH, –NH₂) to a basic group (C=O, –N=) so that an intramolecular hydrogen bond results. This (excited) new form of the molecule returns to the ground state by emitting visible light [18]. This physical property enables numerous applications, such as fluorescent dyes for chemosensors [19–21].

For this purpose, Y. Lin et al. [22] highlighted the optical properties of binuclear complexes of molybdenum^{VI} containing imidazole Mo=O bonds and the dependence of the observed fluorescence wavelength with the electron density between the Mo=O atoms. More recently [23] there are reports in the literature about the synthesis and analysis of fluorescence of molybdenum^V complexes of riboflavin (vitamin B2), which showed a fluorescence maximum at 525 nm using a concentration of 5.32×10^{-5} M in water at 298 °K.

Therefore, with the aim to contribute to this research field, we report the synthesis and the structural characterization of a new complex of molybdenum with a pyridoxal derivative species, as well as the involved reaction mechanisms and the reactivity indexes (DFT) of the initial studies of its fluorescence.

2. Experimental

2.1. Preparation of 4-(1H-benzimidazol-2-yl)-5-(hydroxymethyl)-2-methylpyridin-3-ol hydrochloride (BIMIPY) (1)

Pyridoxal hydrochloride (0.208 g, 1 mmol) was dissolved in 10 mL of anhydrous ethanol. Thereafter, 0.058 g (0.5 mmol) of 1,2-phenylenediamine was added and the mixture was refluxed for 9 h. The orange solid was filtered and washed with cold ethanol (5 mL). The product was recrystallized in a 1:1 ethanol/methanol mixture. Yield: 75%.

Properties: orange, crystalline substance. Melting point: 230–232 °C.

Anal. Calc. for C₁₄H₁₄N₃O₂Cl (291.5): C, 57.63; H, 4.8; N, 14.40. Found: C, 57.63; H, 4.93; N, 14.38%. IR (KBr, cm⁻¹): 3451 [strong, ν(O–H)], 3279 [strong, ν(N–H)], 1618 [middle, ν(C=N)], 1513, 1425 [strong, pyridine ring], 1025 [very strong, ν(C–O)_{alkoh}], 755 [very strong, δ(C=N–H)]. ¹H NMR (400 MHz, DMSO-d₆): δ (ppm) 8.22 (s, 1H, CH),

7.85 (dd, 2H, $^1J_{\text{HH}} = 6.1$, $^2J_{\text{HH}} = 3.2$, Ar), 7.44 (dd, 2H, $^1J_{\text{HH}} = 6.1$ Hz, $^2J_{\text{HH}} = 3.2$ Hz, Ar), 4.88 (s, 2H, CH₂), 2.63 (s, 3H, CH₃).

2.2. Preparation of [(MoO₂)₂(H₂O)₂(μ-O)(BIMIPY-H⁺)₂]·4DMSO·2H₂O (2)

BIMIPY (0.051 g, 0.2 mmol) was dissolved in 8 mL of boiling methanol and then mixed with 0.033 g (0.1 mmol) of bis(acetylacetonato)-dioxidomolybdenum^{VI} dissolved in 5 mL of ethanol. Instantly occurred precipitation of a deep-brown powder. This was filtered, washed with ethanol and dried in vacuum. The solid was dissolved in DMSO at 75°C for 5 min. Light-brown crystals were obtained from this solution. Yield: 45%.

Properties: yellow crystalline substance. Melting point: 200–202 °C.

Anal. Calc. for C₃₂H₃₈N₆O₁₄S₂Mo₂ (986): C, 38.94; H, 3.85; N, 8.51.

Found: C, 38.32; H, 3.91; N, 8.47%. IR (KBr, cm⁻¹): 3453 [s, ν(O–H)], 3271 [s, ν(N–H)], 1621 [s, ν(C=N)], 1555, 1436 [s, pyridine ring], 1017 [vs, ν(C–O)_{alkoh}], 925 [s, ν_{as}(O=Mo=O)], 897 [s, ν(O=Mo=O)_{sym}], 759 [vs, δ(C–N–H)], 415 [w, δ_{as}(O=Mo=O)].

2.3. X-ray structural analyses

A Bruker CCD X8 Kappa APEX II diffractometer operated with graphite monochromator and Mo-Kα radiation (λ = 0.71073 Å) was used for the X-ray structure analyses. The molecular crystal structure of the ligand and the

Mo complex was solved by direct methods with SHELXS [24]. The final structure was refined with SHELXL [24] with anisotropic displacement parameters for all non-hydrogen atoms; hydrogen atoms were refined isotropically as riding atoms at their theoretical ideal positions, with exception of the hydrogen atoms which have been located for the purpose of a discussion of interactions and bonding. Drawings were made with the DIAMOND for Windows [25]. More details about the structure determinations are given in Table S1 (Electronic Supplementary Information).

2.4 Absorption and fluorescence spectroscopic measurements

Photo physical properties of the ligand and complex were investigated in methanol/CHCl₂ (50:50 v/v) solution at room temperature (25.0 ± 0.1°C). The absorption spectra were recorded in quartz cells with 1 cm optical path length using a UV-Vis spectrometer (Varian CARY 50-BIO). The fluorescence spectra were recorded at concentration of 1x10⁻⁷ mol L⁻¹ with a Cary Eclipse fluorescence spectrophotometer (Varian) with excitation and emissions slits of 5nm.

2.5. Computational Details

First principles calculations based on the density functional theory (DFT), using the Gaussian 09 package [26], have been performed to determine the reactivity indices associated to the fragment $[\text{MoO}_2^{+2} \text{ BIMIPY-H}^+]^{+1}$, and to study (using the time dependent DFT(TDDFT) [27]) the absorption and fluorescence spectra of the ligand. The hybrid B3LYP functional was used to describe the exchange and correlation functional [28], and the molecular orbitals were represented by linear combinations of the 3-21G split valence atomic basis set [29]. The geometry taken from the X-ray diffraction data was optimized and an analysis of the calculated vibrational spectrum at the equilibrium geometry showed no imaginary frequencies. Local maps of the Fukui function have been obtained as differences between electron densities maps of the relevant charge states of each studied system. For the study of the spectroscopic response of the ligand, since the experiments were conducted at a 50:50 (v-v) methanol/dichloromethane solution, the TDDFT calculations were made using the Polarizable Continuum Model (PCM) [30], with the resultant dielectric constant of the mixed solvent, 18.289, obtained using the Looyenga's formula [31]. The plots of the calculated spectra were obtained by a lorentzian fit of the calculated excitation/de-excitation transition energies and their respective oscillator strengths. The molecular orbitals and Fukui function maps were generated through the ChemCraft package [32].

3. Results and discussion

3.1. Structural description

Functionalized benzimidazoles represent an important class of N-containing heterocyclic compounds and have received considerable attention in recent times because of their applications as antiulcers, antihypertensives, antivirals, antifungals, anticancers and antihistamines among others [33]. Benzimidazole compounds have been known as promising biologically active agents. The fact that 5,6-dimethylbenzimidazole is a component of natural vitamin B12 triggered the interest of researchers toward benzimidazole derivatives [34]. Fig. 1 represents the structure of the ligand BIMYPY (**1**) as well as the secondary hydrogen interactions occurring in the free hydrochloride form (For Table S2, with selected distances and angles of **1**, see Electronic Supplementary Information).

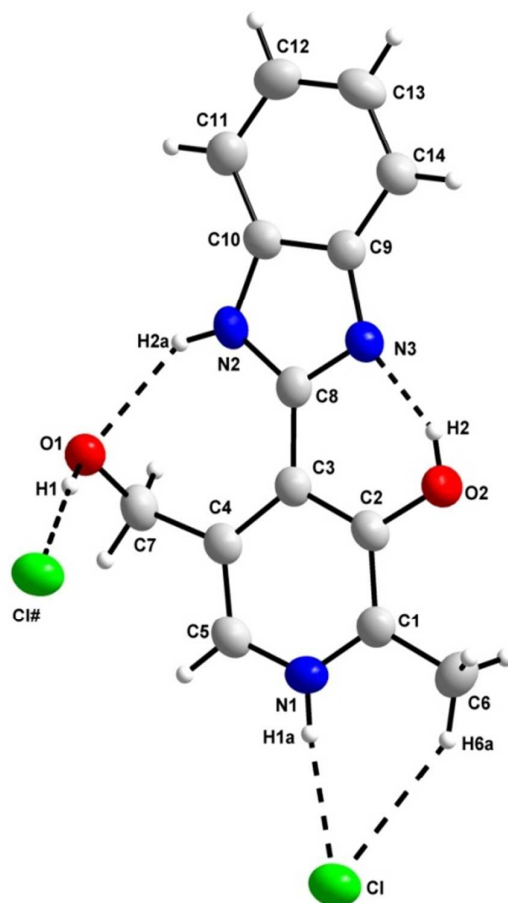


Figure 1. Representation of the molecular structure of the ligand BIMIPY (**1**) and secondary hydrogen interactions (dashed lines).

The dihedral angles between the phenolate and benzimidazole moieties for BIMIPY indicate a nearly planar molecular structure for **1**. This evidence is confirmed by the values of the interplanar angles with the 5-membered ring, showing a torsion angle of only 0.53° out of the plane. Bond lengths and angles in **1** present normal values and are comparable with those reported for related structures [35,36]. The C=N bond distances in the

benzimidazole core are 1.328(3) {C8–N2} and 1.359(5) Å {C8–N3}, intermediate values between a CN single bond (1.40 Å) and a CN double bond (1.28 Å). These bond lengths and the angle attained between the atoms N2–C8–N3 {110.8(2)°} evidence the formation of a benzimidazole ring. Moreover, it is also evident in Fig. 1 the occurrence of intramolecular interactions between hydrogen atoms and nitrogen, oxygen and chlorine. This behavior reflects the intricate packing of salt ions. In fact, donors and acceptors of hydrogen bonds such as R–NH⁺, Cl[–], –C=O and C=N–R fragments can provide a good basis for crystal engineering, in specific of assemblies based upon bifurcated hydrogen bonds [37–38].

In the solid state BIMIPY (**1**) shows intramolecular hydrogen bonds between the phenolic and the imino group [H2⋯N3 = 1.730(4) Å], between the N–H group of the benzimidazole ring and the oxygen atom of the alcoholic group [H2a⋯O1 = 2.249(9) Å] as well as an intermolecular hydrogen bond between the alcoholic group and the chloride ion [H1⋯Cl# = 2.184(8) Å] (Fig. 1). There is another important bifurcated intramolecular hydrogen bonding in evidence, with atoms H6a⋯Cl [2.810(5) Å] and H1a⋯Cl [2.242(2) Å]. The principal secondary interactions occurring in **1** can be seen in Table S3 (Electronic Supplementary Information).

The binuclear complex $[(\text{MoO}_2)_2(\text{H}_2\text{O})_2(\mu\text{-O})(\text{BIMIPY-H}^+)_2]\cdot 2\text{DMSO}\cdot 2\text{H}_2\text{O}$ (**2**) crystallizes in the triclinic space group $P\bar{1}$. A projection of the molecular structure with an atom-labeling scheme is shown in Fig. 2. In **2**, the metal centers attain a distorted octahedral geometry; a water molecule coordinates to each Mo atom and two imidazolic ligands (C=N) imino nitrogen atoms and the oxygen atoms of the deprotonated hydroxyl groups chelate two dioxidomolibdenum(VI) ions (MoO_2^{+2}). As expected, the two Mo=O double bonds are shorter {Mo=O1 = 1.703(7), Mo=O2 = 1.707(7) Å}, than the chelating phenol and H₂O oxygen atoms, respectively Mo–O4 {2.329(2)} and Mo–O5 {2.051(6) Å}. The sixth coordination position in complex **2** is accomplished by a μ -oxido ligand, which connects two moieties $\text{C}_{16}\text{H}_{20}\text{MoN}_3\text{O}_5$ to a dinuclear species, as shown in Fig. 3. This oxido bridge has distances of 1.885(1) Å, with an inversion center, and supports the dimeric configuration of compound **2**. The Mo–O bonds are shorter than the Mo–N {2.197(8) Å} ones, and this can be assigned to the harder basic character of the oxygen atom in respect to nitrogen. Selected bond distances and angles of **2** are listed in Table S2 (Electronic Supplementary Information).

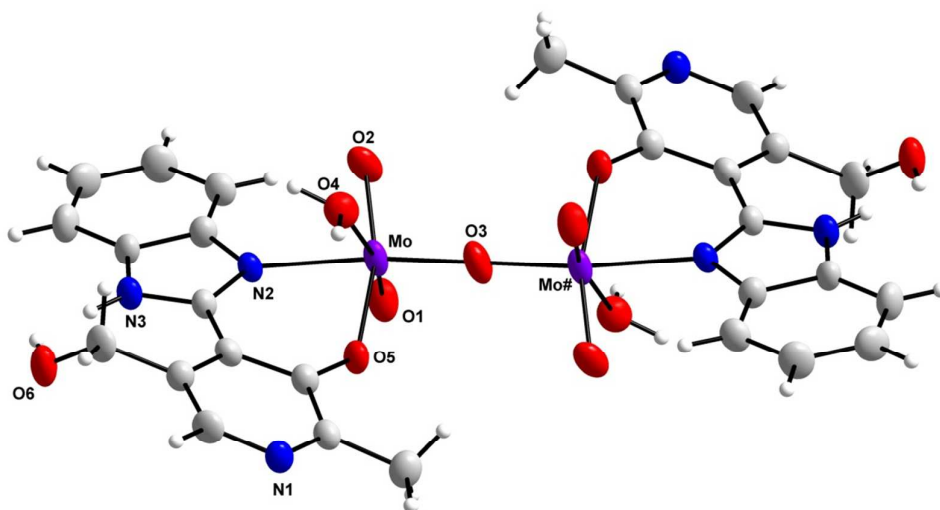


Figure 2. Molecular structure of the molybdenum complex **2** in a thermal ellipsoid representation. The solvates are not shown. Symmetry operations used to generate equivalent atoms: (#) $2-x, 1-y, 2-z$.

The representation of complex **2** along the ab plane, depicted in Fig. 3, allows the visualization of a further intermolecular hydrogen interaction, between the atoms $O4-H4b\cdots N1\#3$ (and $O4\#3-H4b\#3\cdots N1$) {D–H 0.989(1) Å; H \cdots A 1.778(7) Å; D \cdots A 2.742(7) Å; D–H \cdots A 164.56(25) $^\circ$ }. These intermolecular bonds support the growth of the supramolecular assembly of the Mo complex, as shown in Fig. 3 (symmetry transformations used to generate equivalent atoms: (#3) $2-x, -y, 2-z$).

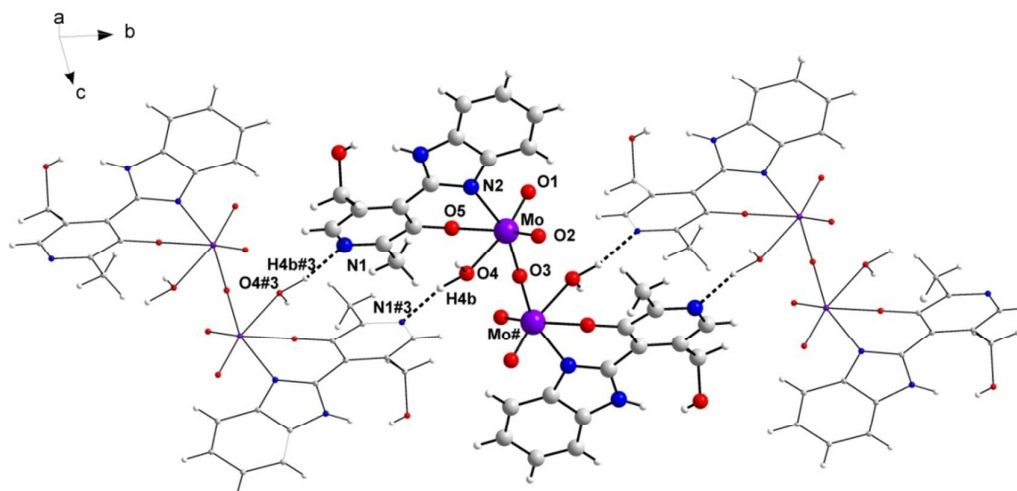


Figure 3. Representation of the D-H...A secondary interactions for the complex **2** along the crystallographic *ab* plane. Symmetry transformations used to generate equivalent atoms: (#3) $2-x, -y, 2-z$.

Changing the view to the *ab* crystallographic plane, as displayed in Fig. 4, it is possible to verify the existence of highly polar layers containing the organic DMSO solvates of crystallization. The incorporation of organic species through the process of recrystallization results in the intercalation of these molecules in the lamellar network of the inorganic host. The water molecules are located closer to the complexes, considerably distant from the layer of dimethylsulfoxide. This process of crystallization, together with the structural conformation of the complex of molybdenum, allowed the opportunity to guide and determine interspersed species, a process that

will be further investigated, to check if other organic solvates can influence the crystallization course and so change the electronic and optical properties of the parent complex.

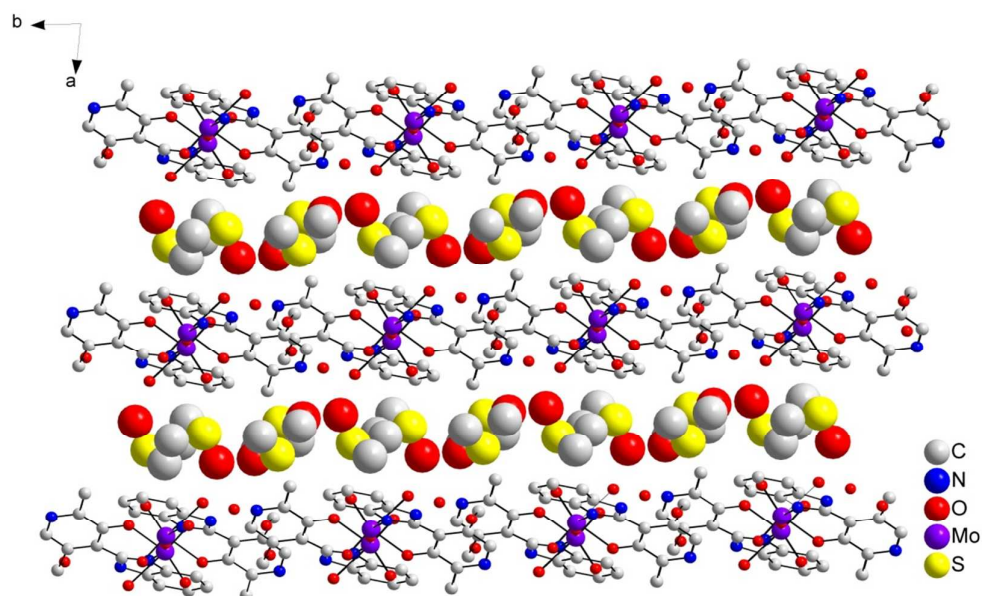
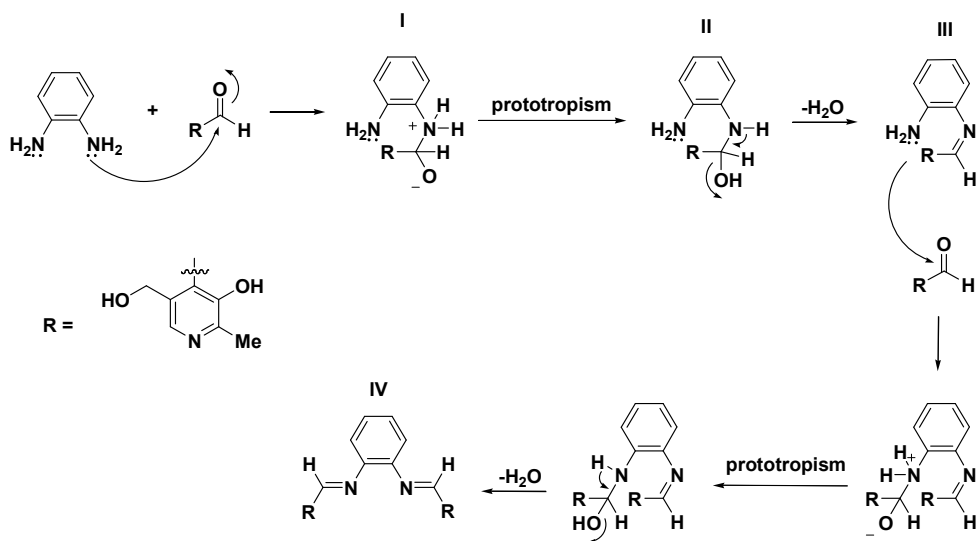


Figure 4. Representation of the layers of crystallization of **2** along the plane *ab*.

3.2 Reactivity indexes for the formation of dimeric molybdenum complex from BIMIPY.

The reaction steps involved in the preparation of the compounds referred in this work are summarized in Chart A.

amine nitrogen atom to form the intermediate **IV**. This mechanism is called nucleophilic addition to carbonyl, addition-elimination type.

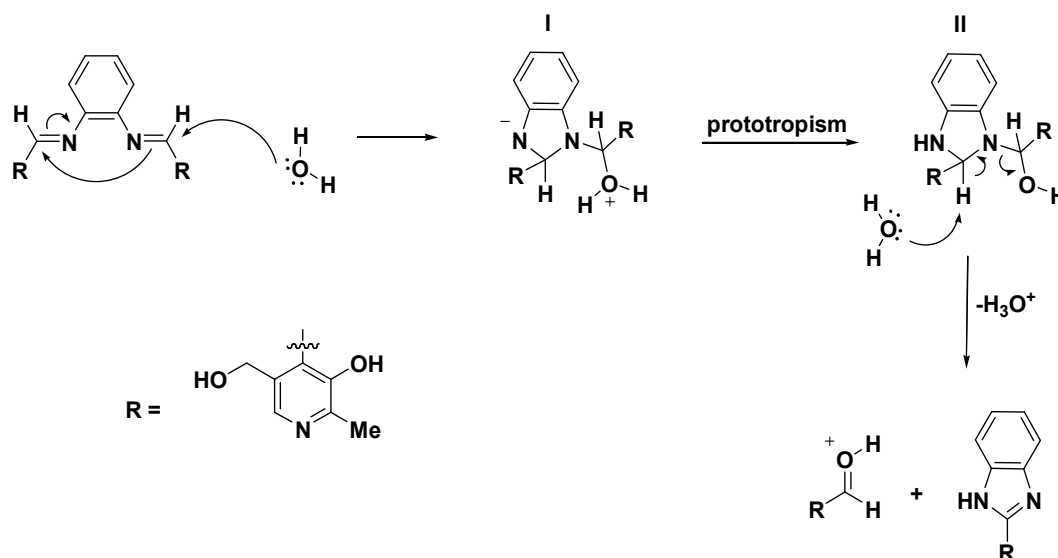


Scheme 1. First step: formation of the intermediary imine.

The further reaction mechanism proposed by us for the formation of the benzimidazole BIMIPY is resumed in Scheme 2 and has the above discussed first step as a concerted mechanism.

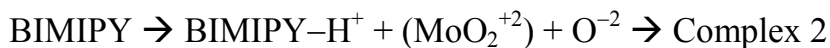
- (i) Initially, a water molecule, previously eliminated, performs a nucleophilic attack to the carbon atom of the imine, promoting the migration of the carbon π electrons to the carbon atom of the other vicinal imine, thus, leading to the formation of the five-membered ring (intermediate) **I**;
- (ii) the further occurrence of prototropism in **I** forms the neutral

intermediary **II**; the second water molecule, also eliminated earlier, acts as a base abstracting a proton to the formation of the π bond, promoting the elimination of one molecule of aldehyde and the formation of the desired benzimidazole. Since the aldehyde was eliminated in the protonated form (more reactive), it reacts further with 1,2-phenylenediamine.



Scheme 2. Second step: mechanism of formation of BIMIPY

Assuming that the formation mechanism of BIMIPY proposed in the reaction schemes **1** and **2** has actually occurred, we now analyze the reaction steps leading to the dimeric molybdenum complex **2** in terms of reactivity indexes, namely, the local Fukui functions [40] for three steps, starting from the BIMIPY molecule until the whole complex **2**:



The Fukui function of a given system, $f(\vec{r})$, can be defined as [27,40]

$$f(\vec{r}) = \left[\frac{\partial \rho(\vec{r})}{\partial N} \right]_{\mathbf{v}}$$

where, $\rho(\vec{r})$, is the electronic density and N is the total number of electrons, for some fixed external potential, \mathbf{v} . The derivative can be approximated by finite differences, and the electrophilic, $f^+(\vec{r})$, and nucleophilic, $f^-(\vec{r})$, regions of a molecule (when subjected to nucleophilic and electrophilic attacks, respectively) are then determined by

$$f^+(\vec{r}) = \rho^{N+1}(\vec{r}) - \rho^N(\vec{r})$$

$$f^-(\vec{r}) = \rho^N(\vec{r}) - \rho^{N-1}(\vec{r})$$

Step 1: Fig. 5 shows the electrophilic regions of BIMIPY and deprotonated BIMIPY. It is clear from this figure that the deprotonation significantly increases the reactivity at the oxygen site under nucleophilic attacks, as should be expected, due to the high electronegativity of oxygen. It gives support to the suggested mechanism where the deprotonation is followed by the incorporation of MoO_2^{+2} .

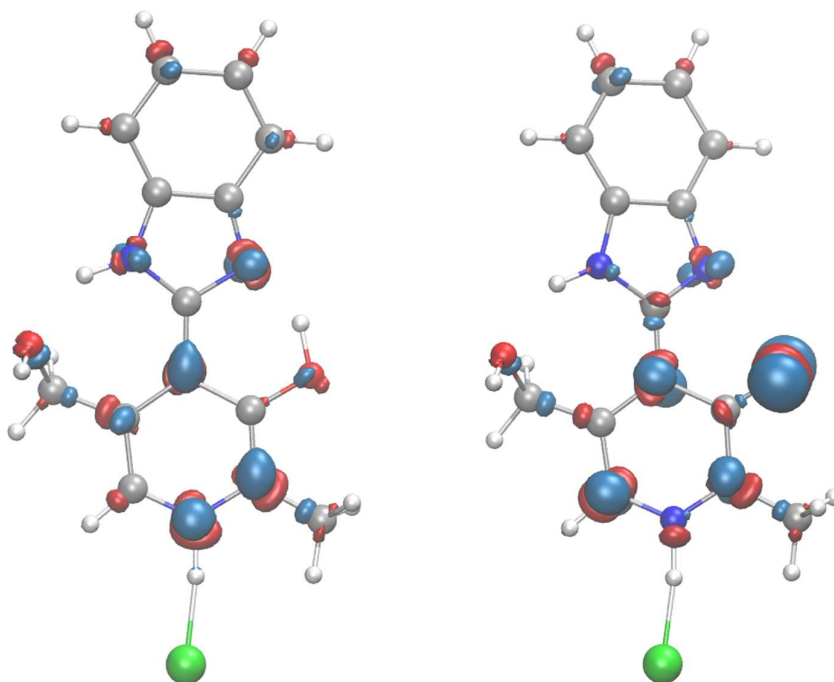


Figure 5. Calculated Fukui function maps of the electrophilic regions of BIMIPY at the left side, and deprotonated BIMIPY at the right side.

Step 2: Once the $\text{BIMIPY}+(\text{MoO}_2^{+2})$ molecule is formed (see Fig. 6), it would be interesting to analyze the reactivity of this molecule against electrophilic attacks, since the next step to form complex 2 would be the incorporation of an oxido ligand, which works as a bridge connecting the identical $\text{BIMIPY}-\text{H}^+ + (\text{MoO}_2^{+2})$ species. The nucleophilic regions of the $\text{BIMIPY}-\text{H}^+ + (\text{MoO}_2^{+2})$ groups are shown in Fig. 6. It is clear that the Mo atom is the most reactive against electrophilic attacks, as in the case of an oxido ion approaching the molecule.

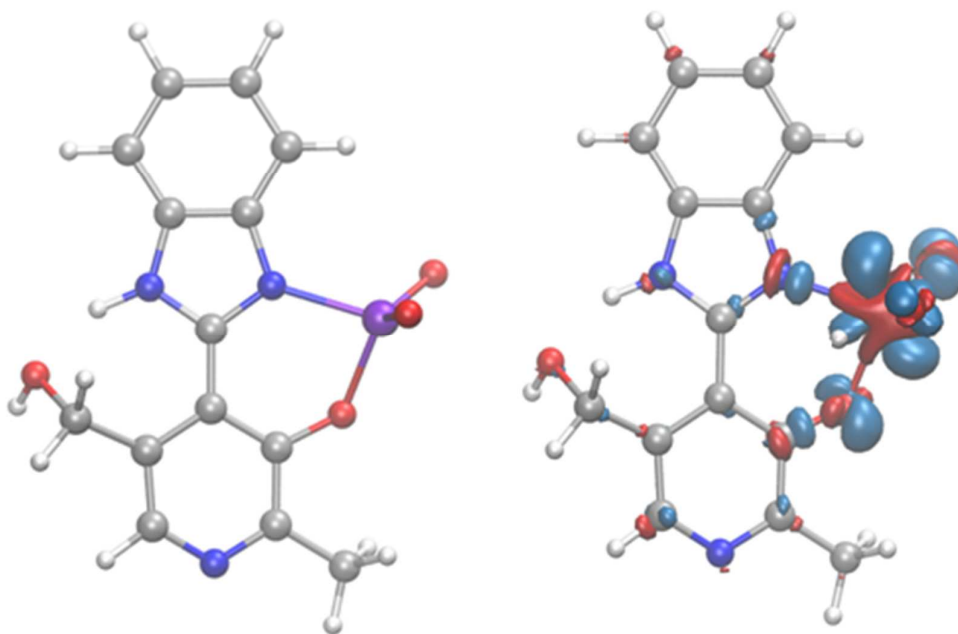


Figure 6. Optimized structure of the BIMIPY-H⁺ + (MoO₂⁺²) molecule at the left side, and its nucleophilic regions, at the right side. The illustration shows only the fragment [MoO₂⁺² BIMIPY-H⁺]⁺¹.

Step 3: Finally, once the O “bridge” atom is incorporated, the last step to form the dimeric complex **2** would be the bonding of the O bridge atom to the second BIMIPY-H⁺ + (MoO₂⁺²) molecule. Only for completeness, we show the electrophilic regions of the BIMIPY-H⁺ + (MoO₂⁺²) + O⁻² molecule in Fig. 7. As should be expected, the most electrophilic regions are concentrated at the oxygen bridge atom, which completes the reactivity scenario leading from the BIMIPY molecule to the dimeric complex **2**.

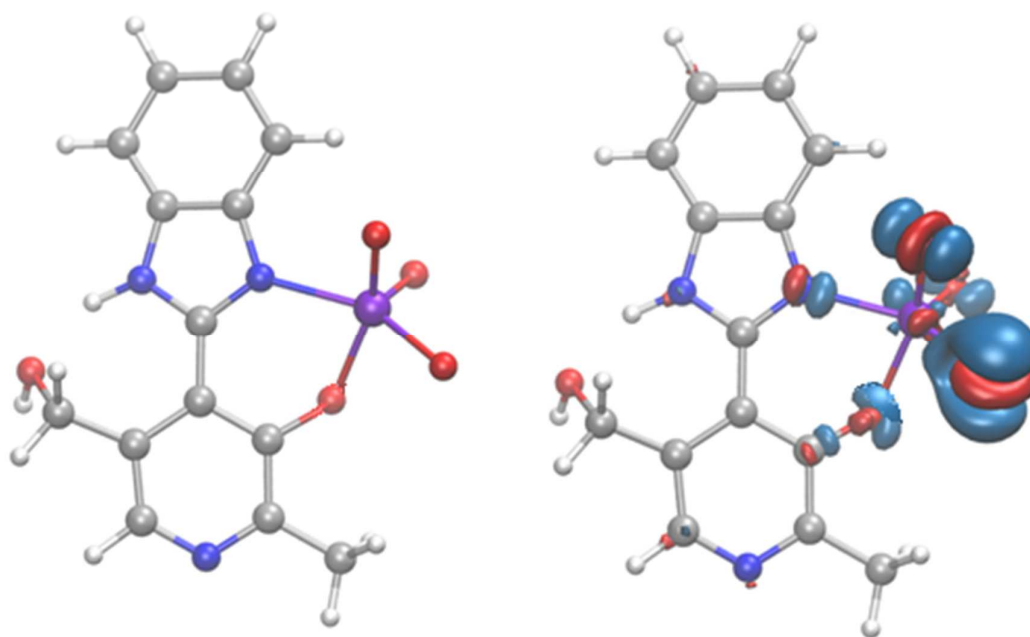


Figure 7. Optimized structure of the BIMIPY+(MoO₂⁺²)+O⁻² molecule at the left side, and its electrophilic regions at the right side.

3.3 Photophysical Properties

3.3.1 Experimental results

The UV-Vis and luminescence spectra of the ligand are showed in Figs. 8 and 9 at room temperature, respectively. The ligand displayed two broad absorption bands at 312 and 386 nm. The molar absorption coefficient determined for the ligand at 386nm was 6296 mol⁻¹ L⁻¹ cm⁻¹. Besides these main bands additional bands can be seen at 222 and 254nm, and a shoulder at 345 nm. Furthermore, it was found that the ligand exhibit intense blue photoluminescence with emission maxima at 471 nm and a shoulder at 410 nm upon excitation at 364 nm. However, spectrofluorimetric measurements

of the complex showed that it does not display fluorescence in solution of methanol/ CH_2Cl_2 (50:50 v/v) at room temperature.

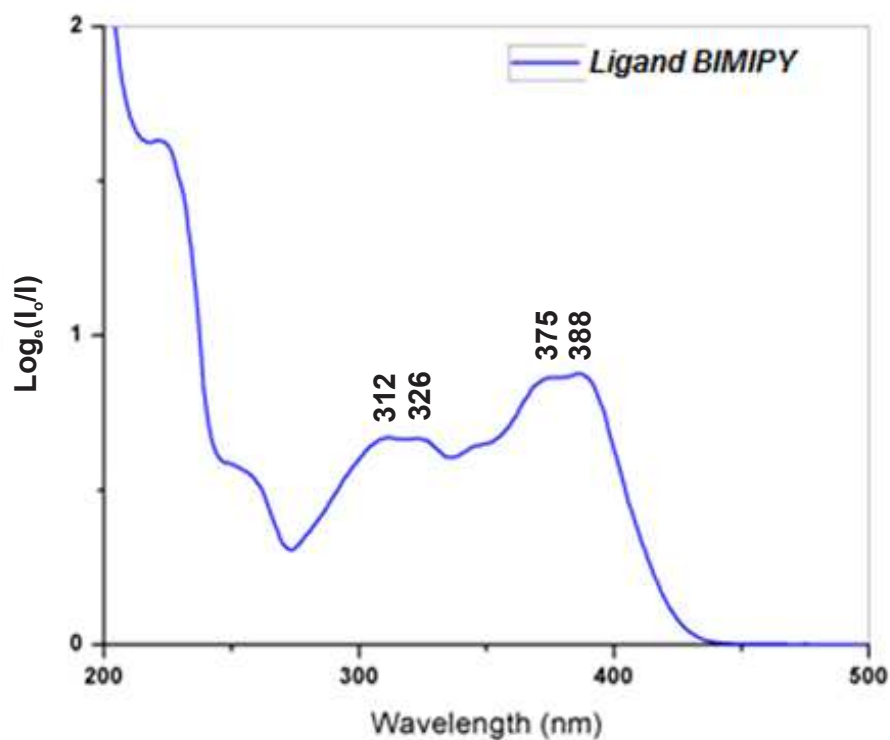


Figure 8. Absorption spectrum of the ligand in solution of methanol/ CH_2Cl_2 at a concentration of $1.22 \times 10^{-4} \text{ mol L}^{-1}$.

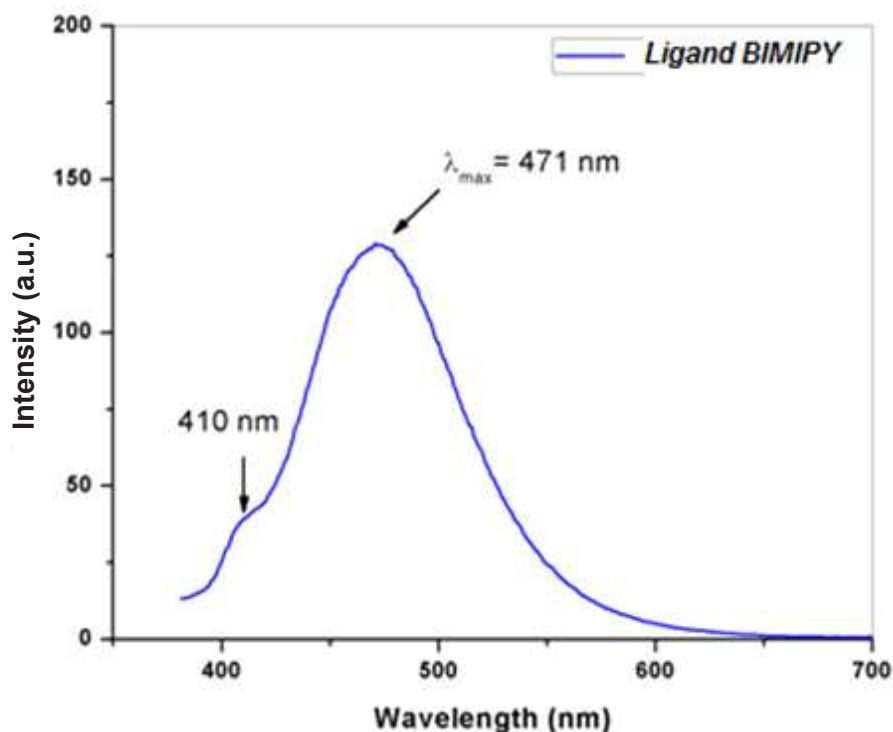


Figure 9. Fluorescence spectrum of the ligand in solution of methanol/ CH_2Cl_2 at a concentration of $1 \times 10^{-7} \text{ mol L}^{-1}$.

3.3.2 Time Dependent DFT results

Time Dependent Density Functional Theory (TDDFT) calculations were performed to obtain information about the main electronic transitions and to assign the fluorescence emission bands of the ligand. The absorption (UV-Vis) (Fig. 10) and fluorescence (Fig. 11) spectra obtained through TDDFT are in good agreement with the experimental spectra (see Figures 8 and 9, respectively). In Figs. 10 and 11, besides the full spectra (in solid lines), it is also shown their decompositions into the contributing

transitions. The electronic transition with the highest oscillator strength of the calculated absorption spectrum occurs at 384.36 nm (to be compared to the experimental 386 peak). The second most intense electronic transition occurs at 287.64 nm, with a wavelength a little shorter than the experimentally observed peaks at higher energy, which is seen at 312 nm. Transitions with lower oscillator strengths are seen at 342.40 nm, which can be identified with the shoulder at 345 nm in the experimental spectrum. A very small peak is also identified at 492.83 nm. Figure 12 shows the molecular orbitals involved in the most intense transition of the absorption spectrum. It can be seen from this Figure that the electronic transition occurs inside the pyridoxal group. The electron is transferred from an anti-bonding π -like orbital (HOMO-3), with a major contribution from the oxygen atom of the pyridoxal, to an anti-bonding π -like orbital (LUMO) centered at the nitrogen atom, and one orbital of its carbon neighbors.

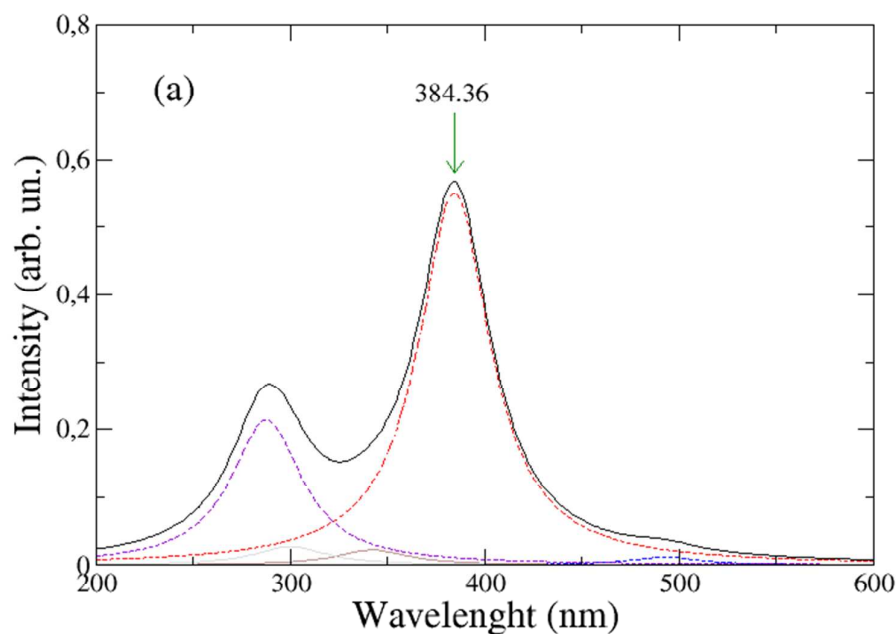


Figure 10. Absorption spectrum of the ligand simulated by using TDDFT in methanol/ CH_2Cl_2 . The solid line shows the full spectrum while the other lines represent the contributing individual transitions.

The fluorescence spectrum of the ligand, as seen in Fig. 11, shows two peaks close to each other, at 416.52 and 453.36 nm, which should be compared to the experimental peaks at 410 and 471 nm, respectively. Another peak at higher energy (308 nm) is also shown. As shown in Fig. 13, the de-excitation electronic transitions occur through the transition of an electron from the LUMO orbital, to π -like orbitals at the oxygen atom of the pyridoxal group. The most intense of these two transitions (at 453.36 nm) involves the same orbitals as in the most intense peak of the absorption spectrum, but now the electron is transferred from the LUMO to the

HOMO-3. The transition at 416.52 nm occurs from the LUMO to the HOMO-4, which is π orbital of the oxygen atom that is directed along the plane of the pyridoxal ring. As said before, no fluorescent activity is experimentally observed for the complex. Further, the optical activity of the ligand is totally concentrated in the pyridoxal group, showing no relevant contribution from the benzimidazole ring.

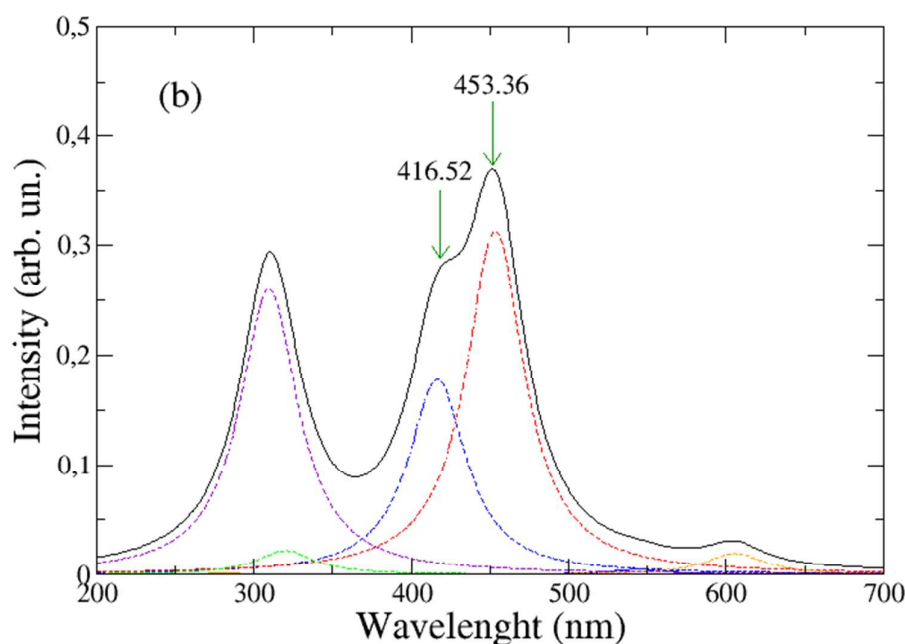


Figure 11. Fluorescence spectra of the ligand simulated by using TDDFT in methanol/ CH_2Cl_2 . The solid line shows the full spectrum while the other lines represent the contributing individual transitions.

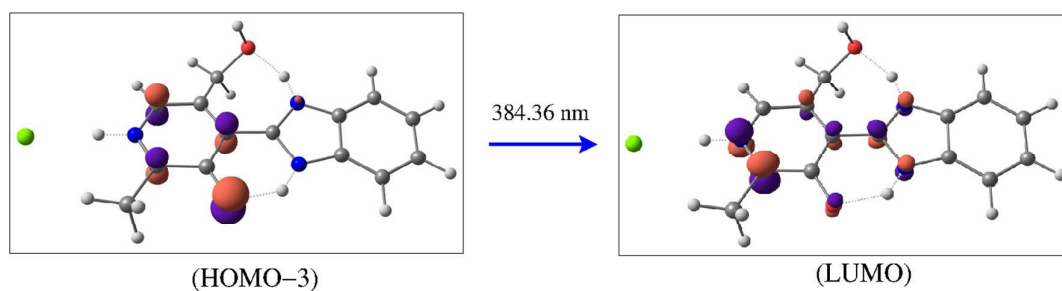


Figure 12. Plots of the orbitals involved in the more intense electronic transition, at 384 nm, of the absorption spectrum of the ligand.

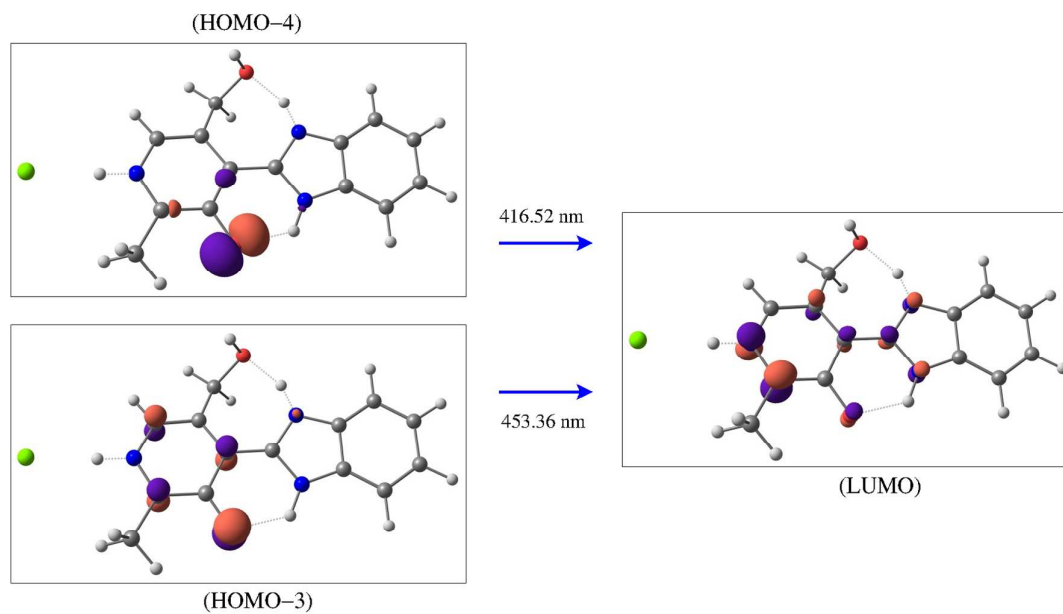


Figure 13. Plots of the orbitals involved in the two major peaks, at 416 and 453 nm, of the fluorescence spectrum of the ligand.

4. Conclusions

Organic species which contain imidazolic rings as ligands – like pyridoxal – are of great interest because they combine the metabolic potential of the vitamin B6 family with the chemical ability to form stable chelate complexes. Up to date no other references have been made to the complexation of molybdenum by any other similar vitamin B6 constituent. The proposed complexation mechanism has been corroborated through FPDFT theory in the determination of the reactivity sites of the fragments taking place in the complexation steps. For example, the reactivity of the species $\text{BIMIPY}+(\text{MoO}_2^{+2})$ against electrophilic attack was analyzed, since the next reaction step in the formation of complex **2** should be the incorporation of an oxido ligand, which achieves a bridge between the identical $\text{BIMIPY}-\text{H}^+ + (\text{MoO}_2^{+2})$ species to form complex **2**. FPDFT theory was also employed in fluorescence studies of the ligand: the fluorescence activity was shown to be completely localized inside the pyridoxal group of the BIMIPY ligand.

Appendix A. Supplementary data

CCDC 861363 and 861364 contain the supplementary crystallographic data for compounds **1** and **2**. These data can be obtained free of charge via <http://www.ccdc.cam.ac.uk/conts/retrieving.html>, or from the Cambridge

Crystallographic Data Centre, 12 Union Road, Cambridge CB2 1EZ, UK;
fax: (+44) 1223-336-033; or e-mail: deposit@ccdc.cam.ac.uk.

Acknowledgement

Brazilian Research Councils CNPq – Edital N° 14/2011. FAPERGS -
Fundação de Amparo à Pesquisa do Estado do Rio Grande do Sul - Edital
N° 002/2011 – PQG

References

- [1] J. Olivard, D.E. Metzler, E.E. Snell, *J. Biol. Chem.* 199 (1952) 669–674.
- [2] D.E. Metzler, J.B. Longenecker, E.E. Snell, *J. Am. Chem. Soc.* 76 (1954) 639–644.
- [3] S. Wei, J. Wang, S. Venhuizen, R. Skouta, R. Breslow, *Bioorg. Med. Chem. Lett.* 19 (2009) 5543–5546.
- [4] Y.-L. Lin, J. Gao, A. Rubinstein, D.T. Major, *Biochim. Biophys. Acta* 1814 (2011) 1438–1446.
- [5] L.T.T. Bui, D.M. Small, *Food Chemistry* 130 (2012) 841–846.
- [6] H. Ikushiro, H. Hayashi, *Biochim. Biophys. Acta* 1814 (2011) 1474–1480.

- [7] Y. Fujitani, N. Nakajima, K. Ishihara, T. Oikawa, K. Ito, M. Sugimoto, *Phytochemistry* 67 (2006) 668–674.
- [8] A.J Kesel, *Bioorg. Med. Chem.* 11 (2003) 4599–4613.
- [9] J.-J Jiang, T.C. Chang, W. Hsu, J.-M. Hwang, L.-Y. Hsu, *Chem. Pharm. Bull.* 51 (2003) 1307–1310.
- [10] J.S. Casas, A. Castiñeiras, F. Condori, *Polyhedron* 22 (2003) 53–65.
- [11] J.C Pessoa, I. Correia, M.T. Duarte, *Chem. Eur. J.* 10 (2004) 2301–2317.
- [12] E. Bonfada, G. Manzoni de Oliveira, D.F. Back, E. Schulz Lang, *Z. Anorg. Allg. Chem.* 631 (2005) 878–881.
- [13] G. Manzoni de Oliveira, D.F. Back, E. Schulz Lang, *J. Inorg. Biochem.* 100 (2006) 1698–1704.
- [14] G. Manzoni de Oliveira, D.F. Back, É. Bonfada, E. Schulz Lang, *J. Inorg. Biochem.* 101 (2007) 709–714.
- [15] G. Manzoni de Oliveira, D.F. Back, J.P. Vargas, E. Schulz Lang, G. Tabarelli, *J. Inorg. Biochem.* 102 (2008) 666–672.
- [16] G. Manzoni de Oliveira, D.F. Back, E. Schulz Lang, J.P. Vargas, *Polyhedron* 27(2008) 2551–2556.
- [17] D.F. Back, G. Manzoni de Oliveira, M.A. Ballin, V.A. Corbellini, *Inorg. Chim. Acta* 363 (2010) 807–812.

- [18] S. P. De, S. Ash, S. Dalai, A. Misra. *Journal of Molecular Structure: THEOCHEM* 807 (2007) 33–41.
- [19] Y. Yang, B. Li, L. Zhang, Y. Guan. *Journal of Luminescence* 145 (2014) 895–898.
- [20] M. Hranjeca, E. Horak, M. Tireli, G. Pavlović, G. Karminski-Zamola. *Dyes and Pigments* 95 (2012) 644–656.
- [21] D. Y. Lee, N. Singh, D. O. Jang. *Tetrahedron Letters* 52 (2011) 1368–1371.
- [22] Y-W Li, Y-P Tong, C Yang, Y- Lin. *Bioorganic & Medicinal Chemistry Letters* 12 (2002) 869–871.
- [23] C. N. Malele, J. Ray, W. E. Jones Jr. *Polyhedron* 29 (2010) 749–756.
- [24] G.M. Sheldrick, *Acta Cryst. A*64 (2008) 112–122.
- [25] K. Brandenburg, *DIAMOND 3.1a*. 1997 – 2005, Version 1.1a. Crystal Impact GbR, Bonn, Germany.
- [26] Gaussian 09, Revision C.01, M. J. Frisch, G. W. Trucks, H. B. Schlegel, G. E. Scuseria, M. A. Robb, J. R. Cheeseman, G. Scalmani, V. Barone, B. Mennucci, G. A. Petersson, H. Nakatsuji, M. Caricato, X. Li, H. P. Hratchian, A. F. Izmaylov, J. Bloino, G. Zheng, J. L. Sonnenberg, M. Hada, M. Ehara, K. Toyota, R. Fukuda, J. Hasegawa, M. Ishida, T. Nakajima, Y. Honda, O. Kitao, H. Nakai, T. Vreven, J. A. Montgomery, Jr., J. E. Peralta, F. Ogliaro, M. Bearpark, J. J. Heyd, E. Brothers, K. N.

Kudin, V. N. Staroverov, R. Kobayashi, J. Normand, K. Raghavachari, A. Rendell, J. C. Burant, S. S. Iyengar, J. Tomasi, M. Cossi, N. Rega, J. M. Millam, M. Klene, J. E. Knox, J. B. Cross, V. Bakke, C. Adamo, J. Jaramillo, R. Gomperts, R. E. Stratmann, O. Yazyev, A. J. Austin, R. Cammi, C. Pomelli, J. W. Ochterski, R. L. Martin, K. Morokuma, V. G. Zakrzewski, G. A. Voth, P. Salvador, J. J. Dannenberg, S. Dapprich, A. D. Daniels, O. Farkas, J. B. Foresman, J. V. Orti, J. Cioslowski, and D. J. Fox, Gaussian, Inc., Wallingford CT, 2009.

[27] a) E. Runge, E. K. U. Gross, *Phys. Rev. Lett.* 52 (1984) 997–1000; b) M. E. Casida, in “Recent Advances in Density Functional Methods”, D. P. Chong (Ed.), World Scientific: Singapore, 1995.

[28] a) A. D. Becke, *J. Chem. Phys.* 98 (1993) 1372–1377;

b) C. Lee, W. Yang, R. G. Parr, *Phys. Rev. B* 37 (1988) 785–789.

[29] a) J. S. Binkley, J. A. Pople, and W. J. Hehre, *J. Am. Chem. Soc.* 102 (1980) 937–947; b) K. D. Dobbs, W. J. Hehre, *J. Comp. Chem.* 8 (1987) 880–893.

[30] J. Tomasi, B. Mennucci, and R. Cammi, “Quantum mechanical continuum solvation models”, *Chem. Rev.* 105 (2005) 2999–3093.

[31] H. Looyenga, *Physica.* 31 (1965) 401–406.

[32] <http://www.chemcraftprog.com>

- [33] P. Ghosh, A. Mandal, *Catalysis Communications* 12 (2011) 744–747.
- [34] F. Xue, X. Luo, C. Ye, W. Ye, Y. Wang, *Bioorg. Med. Chem.* 19 (2011)2641–2649.
- [35] Y.-P. Tong, S.-L. Zheng, X.-M. Chen, *Eur. J. Inorg. Chem.* (2005) 3734–3741.
- [36] X. Quezada-Buendía, A. Esparza-Ruiz, A. Peña-Hueso, N. Barba-Behrens, R. Contreras, A. Flores-Parra, S. Bernès, S.E. Castillo-Blum, *Inorg. Chim. Acta* 361 (2008) 2759–2767.
- [37] G.R. Desiraju, T. Steiner, *Structural Chemistry and Biology: The Weak Hydrogen Bond (International Union of Crystallography - Monographs on Crystallography)*, Oxford University Press, 2001.
- [38] G. Manzoni de Oliveira, D.F. Back, M. Hörner, F. Broch, *Polyhedron* 31 (2012) 558–564.
- [39] X. Yang, R.A. Jones, R.J. Lai, A. Waheed, M.M. Oye, A.L. Holmes, *Polyhedron* 25 (2006) 881–887.
- [40] R. G. Parr, W. Yang, *Density-Functional Theory of Atoms and Molecules (International Series of Monographs on Chemistry)* Oxford University Press, 1989.

New Journal of Chemistry – Table of Content

Studies based on FPDFT helped us to elucidate the reaction mechanism involving the $\text{BIMIPY-H}^+ + (\text{MoO}_2^{+2})$ species in the first complexation of molybdenum by a vitamin B6 constituent.

